Inorganic Chemistry

ARTICLE

pubs.acs.org/IC

Synthesis, Characterization, and Structure−Property Relationships in Two New Polar Oxides: $Zn_2(MoO_4)(SeO_3)$ and $Zn_2(MoO_4)(TeO_3)$

Sau Doan Nguyen, Sang-Hwan Kim, and P. Shiv Halasyamani*

Department of Chemistry, University of Houston, 136 Fleming Building, Houston, Texas 77204-5003, United States

Supporting Information

ABSTRACT: Two new noncentrosymmetric (NCS) polar oxide materials, $Zn_2(MoO_4)(AO_3)$ (A = Se^{4+} or Te^{4+}), have been synthesized by hydrothermal and solid-state techniques. Their crystal structures have been determined, and characterization of their functional properties (second-harmonic generation, piezoelectricity, and polarization) has been performed. The isostructural materials exhibit a three-dimensional network consisting of ZnO_4, ZnO_6, MoO_4, and AO_3 polyhedra that share edges and corners. Powder second-harmonic generation (SHG) measurements using 1064 nm radiation indicate the materials exhibit moderate SHG efficiencies of 100 × and 80 × α-SiO_2 for $Zn_2(MoO_4)(SeO_3)$ and $Zn_2(MoO_4)(TeO_3)$, respectively. Particle size vs SHG efficiency measurements indicate the materials are type 1 non-phase-matchable. Converse piezoelectric measurements resulted in d_{33} values of ∼14 and ∼30 pm/V for $Zn_2(MoO_4)(SeO_3)$ and $Zn_2(MoO_4)(TeO_3)$, respectively, whereas pyroelectric measurements revealed coefficients of −0.31 and −0.64 $\mu C/m^2$ K at 55 °C for $Zn_2(MoO_4)(SeO_3)$ and $Zn_2(MoO_4)(TeO_3)$, respectively. Frequency-dependent polarization measurements confirmed that all of the materials are nonferroelectric; that is, the macroscopic polarization is not reversible, or "switchable". Infrared, UV−vis, thermogravimetric, and differential thermal analysis measurements were also performed. First-principles density functional theory (DFT) electronic structure calculations were also done. Crystal data: $Zn_2(MoO_4)(SeO_3)$, monoclinic, space group $P2_1$ (No. 4), a = 5.1809(4) Å, b = 8.3238(7) Å, c = 7.1541(6) Å, β = 99.413(1)°, V = 305.2(1) $Å^3$, Z = 2; $Zn_2(MoO_4)(TeO_3)$, monoclinic, space group $P2_1$ (No. 4), a = 5.178(4) Å, b = 8.409(6) Å, c = 7.241(5) Å, β = 99.351(8)°, V = 311.1(4) $Å^3$, Z = 2.

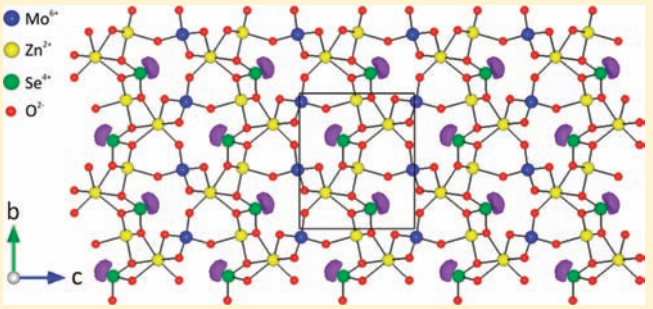

INTRODUCTION

Noncentrosymmetric (NCS) materials are of topical and technological interest attributable to their functional properties, for example, second-harmonic generation (SHG), ferroelectricity, and piezoelectricity.[1−4] A subset of NCS materials are compounds that are polar, that is, materials that exhibit a macroscopic dipole moment. A material is considered polar if it crystallizes in one of 10 polar crystal classes (1, 2, 3, 4, 6, m, mm2, 3m, 4mm, or 6mm).[5] NCS materials may exhibit SHG and piezoelectricity, but *only* polar NCS compounds may be additionally ferroelectric and/or pyroelectric. With ferroelectricity, the observed macroscopic polarization is reversible, or switchable, in the presence of an external electric field,[6] whereas with pyroelectricity the polarization is not reversible, but the magnitude of the polarization varies as a function of temperature.[4] Thus, ferroelectricity is a subset of pyroelectricity. In other words, all ferroelectrics are pyroelectrics, but the converse is not true. With respect to new materials, a number of strategies have been published describing the design and synthesis of new polar materials.[7−23] Our strategy has been to synthesize new polar oxide materials that contain cations susceptible to second-order Jahn−Teller distortions.[24−32] These cations are octahedrally coordinated d^0 transition metals (Ti^{4+}, Nb^{5+}, W^{6+}, etc.) and cations that exhibit a stereoactive lone-pair (Se^{4+}, Te^{4+}, I^{5+}, etc.). In both of these families of cations, the local metal coordination is NCS *and* polar. If the individual polar polyhedra align, macroscopic polarity is observed, and the aforementioned functional properties may be observed. This design strategy has also been exploited successfully in oxyfluoride materials.[13,33,34] We have successfully synthesized and characterized the functional properties of a variety of new polar oxide materials.[35−47] The magnitudes of these functional phenomena are critically dependent on the individual polar polyhedra, as well as the extent of their alignment in the crystal structure.

In this paper, we report on the synthesis, structure, and functional properties of two new polar oxide materials, $Zn_2(MoO_4)(SeO_3)$ and $Zn_2(MoO_4)(TeO_3)$. The polar materials contain a cation with a stereoactive lone-pair, Se^{4+} or Te^{4+}, and a d^0 transition metal, Mo^{6+}. A second-order Jahn−Teller (SOJT) distortion is, however, only observed in the former cations, as the Mo^{6+} cations are in tetrahedral coordination environments. In addition, although both materials are polar, we demonstrate that the polarity is not reversible — the materials are not ferroelectric. Finally, structure−property relationships and theoretical calculations are discussed and presented.

Received: March 11, 2011
Published: May 10, 2011

Table 1. Crystallographic Data for $Zn_2(MoO_4)(AO_3)$ (A = Se^{4+} or Te^{4+})

formula	$Zn_2(MoO_4)(SeO_3)$	$Zn_2(MoO_4)(TeO_3)$
fw (g/mol)	417.64	466.28
T (K)	296.0(2)	296.0(2)
λ (Å)	0.71073	0.71073
crystal system	monoclinic	monoclinic
space group	$P2_1$ (No. 4)	$P2_1$ (No. 4)
a (Å)	5.1809(4)	5.178(4)
b (Å)	8.3238(7)	8.409(6)
c (Å)	7.1541(6)	7.241(5)
α	90	90
β	98.413(1)	99.351 (8)
γ	90	90
V (Å^3)	305.2 (1)	311.1(4)
Z	2	2
ρ_{calcd} (g/cm^3)	4.545	4.978
μ (mm^{-1})	15.765	14.212
$2\theta_{max}$ (deg)	57.8	57.6
R (int)	0.0265	0.0228
GOF (F^2)	1.075	1.099
R (F)[a]	0.0182	0.0212
$R_w(F_o^2)$[b]	0.0437	0.0542
Flack parameter	0.00(3)	0.00(2)

[a] $R(F) = \Sigma||F_o| - |F_c||/\Sigma|F_o|$. [b] $R_w(F_o^2) = [\Sigma w(F_o^2 - F_c^2)^2/\Sigma w(F_o^2)^2]^{1/2}$.

Table 2. Selected Bond Distances (Å) for $Zn_2(MoO_4)(AO_3)$ (A = Se^{4+} or Te^{4+})

$Zn_2(MoO_4)(SeO_3)$		$Zn_2(MoO_4)(TeO_3)$	
Zn(1)−O(1)	1.963(3)	Zn(1)−O(1)	1.937(5)
Zn(1)−O(2)	2.002(3)	Zn(1)−O(2)	1.973(5)
Zn(1)−O(4)	1.968(3)	Zn(1)−O(4)	1.953(5)
Zn(1)−O(7)	1.990(3)	Zn(1)−O(7)	1.998(6)
Zn(2)−O(1)	2.227(3)	Zn(2)−O(1)	2.155(5)
Zn(2)−O(2)	2.184(3)	Zn(2)−O(2)	2.118(5)
Zn(2)−O(3)	2.099(3)	Zn(2)−O(3)	2.181(5)
Zn(2)−O(4)	2.197(3)	Zn(2)−O(4)	2.168(5)
Zn(2)−O(5)	1.986(3)	Zn(2)−O(5)	2.016(5)
Zn(2)−O(6)	2.040(3)	Zn(2)−O(6)	2.079(5)
Se−O(1)	1.717(3)	Te−O(1)	1.882(5)
Se−O(2)	1.705(3)	Te−O(2)	1.887(5)
Se−O(4)	1.721(3)	Te−O(4)	1.890(5)
Mo−O(3)	1.789(3)	Mo−O(3)	1.790(5)
Mo−O(5)	1.755(4)	Mo−O(5)	1.766(6)
Mo−O(6)	1.744(4)	Mo−O(6)	1.743(5)
Mo−O(7)	1.749(3)	Mo−O(7)	1.763(5)

EXPERIMENTAL DETAILS

Reagents. ZnO (Alfa Aesar, 99.9%), SeO_2 (Alfa Aesar, 99.4%), TeO_2 (GFS, 99.6%), MoO_3 (Alfa Aesar, 99.9%) were used as received.

Synthesis. Bulk polycrystalline and crystals of $Zn_2(MoO_4)(SeO_3)$ were prepared by combining 0.163 g (2.00×10^{-3} mol) of ZnO, 0.110 g (1.00×10^{-3} mol) of SeO_2, and 0.144 g (1.00×10^{-3} mol) of MoO_3 The mixture was thoroughly ground and pressed into a pellet, and placed in a fused silica tube that was evacuated and flame-sealed. The sealed ampule was heated to 380 °C for 24 h, to 500 °C for 24 h, and finally to 550 °C for 48 h before being cooled to room temperature at 6 °C h^{-1}. The product consisted of colorless rod-shaped crystals (~10% yield based on ZnO) and white powder. Powder X-ray diffraction (PXRD) data indicated that the crystals and the powder were the same phase (see Figure S1, Supporting Information).

Crystals of $Zn_2(MoO_4)(TeO_3)$ were grown using hydrothermal techniques. 0.163 g (2.00×10^{-3} mol) of ZnO, 0.160 g (1.00×10^{-3} mol) of TeO_2, 0.144 g (1.00×10^{-3} mol) of MoO_3, and 3 mL of NH_4Cl/NH_3 1 M buffer solution were placed in a 23 mL Teflon-lined autoclave that was subsequently closed. The autoclave was heated to 230 °C for 2 days and then cooled slowly to room temperature at a rate of 6 °C h^{-1}. The product consisted of colorless rod-shaped crystals (~30% yield based on ZnO) and white polycrystalline powder. As with the $Zn_2(MoO_4)(SeO_3)$ synthesis, the crystals and white powder were shown to be the same phase by PXRD (see Figure S1, Supporting Information). Polycrystalline $Zn_2(MoO_4)(TeO_3)$ was prepared by combining 0.163 g (2.00×10^{-3} mol) of ZnO, 0.160 g (1.00×10^{-3} mol) of TeO_2, 0.144 g (1.00×10^{-3} mol) of MoO_3. This mixture was ground and pressed into a pellet. The pellet was heated to 550 °C in air for 2 days and cooled to room temperature of 3 °C min^{-1}. The product was then reground and the above process was repeated three times in order to get a single phase. The reaction and purity of the resultant sample were monitored by PXRD until its PXRD pattern was consistent with the PXRD pattern generated from its single crystal structure data (see Figure S1, Supporting Information).

Single Crystal X-ray Diffraction. For $Zn_2(MoO_4)(SeO_3)$, a colorless rod-shaped crystal ($0.04 \times 0.02 \times 0.02$ mm^3) and for $Zn_2(MoO_4)(TeO_3)$, a colorless rod-shaped crystal ($0.06 \times 0.01 \times 0.01$ mm^3), were used for single-crystal X-ray data collection. Data were collected using a Siemens SMART APEX diffractometer equipped with a 1K CCD area detector using graphite-monochromated Mo Kα radiation. A hemisphere of data was collected using a narrow-frame method with scan widths of 0.30° in ω and an exposure time of 40 s per frame. The first 50 frames were remeasured at the end of the data collection to monitor instrument and crystal stability. The data were integrated using the Siemens SAINT program,[48] with the intensities corrected for Lorentz, polarization, air absorption, and absorption attributable to the variation in the path length through the detector face plate. Psi-scans were used for the absorption correction on the hemisphere of data. The data were solved and refined using SHELXS-97 and SHELXL-97, respectively.[49,50] All of the atoms were refined with anisotropic thermal parameters, and the refinement converged for $I > 2\sigma(I)$. All calculations were performed using the WinGX-98 crystallographic software package.[51] The structure was checked for missing symmetry elements using PLATON.[52] The Flack parameters were refined to 0.00(3) and 0.00(2) for $Zn_2(MoO_4)(SeO_3)$ and $Zn_2(MoO_4)(TeO_3)$, respectively. Crystallographic data and selected bond distances for $Zn_2(MoO_4)(SeO_3)$ and $Zn_2(MoO_4)(TeO_3)$ are given in Tables 1 and 2.

Powder X-ray Diffraction. The X-ray powder diffraction data were collected using a PANalytical X'PertPRO diffractometer at room temperature (Cu $K\alpha$ radiation, flat plate geometry) equipped with X'Celerator detector. Data were collected in the 2θ range of 5−70° with a step size of 0.008° and a step time of 0.3 s.

Infrared Spectroscopy. Infrared spectra were recorded on a Matteson FTIR 5000 spectrometer in the spectral range of 400−4000 cm^{-1} at room temperature. The sample (5 mg) was finely ground with dry KBr (100 mg). This powder mixture was then transferred to a stainless steel IR holder and pressed to a semitransparent pellet (~0.2 mm).

UV−vis Diffuse Reflectance Spectroscopy. UV−vis diffuse reflectance spectra were collected with a Varian Cary 500 scan UV−vis−NIR spectrophotometer over the spectral range of 200−2000 nm at room temperature. Polytetrafluoroethylene (PTFE) was used as a standard

material for baseline correction. The sample was thoroughly mixed with PTFE and this mixture was used for UV−vis measurements. Reflectance spectra were converted to absorbance based on the Kubelka−Munk equation.[53,54]

Thermal Analysis. Thermogravimetric and differential thermal analyses were simultaneously carried out on an EXSTAR6000 TG/DTA 6300 thermogravimetric/differential thermal analysis system (SII Nano-Technology Inc.). The sample (∼20 mg) was placed in a platinum crucible that was heated (cooled) at a rate of 10 °C/min in the range of 25−700 °C for $Zn_2(MoO_4)(SeO_3)$ and 25−850 °C for $Zn_2(MoO_4)(TeO_3)$ under flowing nitrogen gas. A platinum crucible containing 20 mg of Al_2O_3 was used as the reference during the measurements.

Second Harmonic Generation. Powder SHG measurements were performed at room temperature on a modified Kurtz-NLO system,[55] using a pulsed Nd:YAG laser with a wavelength of 1064 nm. The methodology and instrumentation details have been published.[2] The SHG efficiency has been shown to be particle size dependent.[55] Thus, the polycrystalline samples were ground and sieved into distinct particle size ranges (20−45, 45−63, 63−75, 75−90, and 90−120 μm). In order to evaluate relative SHG efficiencies of the measured samples with known SHG materials and calculate their average nonlinear optical (NLO) susceptibilities, $\langle d_{eff}\rangle_{exp}$, crystalline α-$SiO_2$ was also ground and sieved into the same particle size ranges. No index matching fluid was used in the experiment.

Piezoelectric Measurements. Converse piezoelectric measurements were performed at room temperature using a Radiant Technologies RT66A piezoelectric test system with a TREK (609E-6) high voltage amplifier, Precision Materials Analyzer, Precision High Voltage Interface, and MTI 2000 Fotonic Sensor. $Zn_2(MoO_4)(SeO_3)$ and $Zn_2(MoO_4)(TeO_3)$ samples were pressed in to pellets (∼10 mm diameter and ∼1 mm thick). The $Zn_2(MoO_4)(SeO_3)$ pellet was placed in a fused silica tube that was evacuated and flame-sealed. Both pellets were sintered at 550 °C for 1 day. Silver paste was applied to both sides of the sintered pellets as electrodes, and the pellets were cured at 300 °C for 72 h in air. These pellets were also used in polarization measurements.

Polarization Measurements. The polarization measurements were done on a Radiant Technologies model RT66A ferroelectric test system with a TREK high-voltage amplifier in the temperature range of 25−185 °C in a Delta model 9023 environmental test chamber. The unclamped pyroelectric coefficient, defined as dP/dT, was determined by measuring the polarization as a function of temperature. The methodology and instrumentation details have been published.[2] To measure the potential ferroelectric behavior, frequency-dependent polarization measurements were done at room temperature under a static electric field of 10−15 kV/cm between 50−1000 Hz. For the pyroelectric measurements, the polarization was measured statically from room temperature to 185 °C in various increments with an electric field of 12 kV/cm and at 100 Hz. The temperature was allowed to stabilize before the polarization was measured.

Computational Details. First-principles density functional theory (DFT)[56,57] electronic structure calculations for $Zn_2(MoO_4)(SeO_3)$ and $Zn_2(MoO_4)(TeO_3)$ were carried out using numerical atomic orbitals (NAO)[58] and planewave (PW) pseudopotential (PP) methods as implemented in SIESTA[59,60] (3.0-rc2 version)[61] and Quantum ESPRESSO (4.1.2 version)[62] packages, respectively. For the NAOPP calculations in SIESTA, norm-conserving Martins-Troullier (MT) pseudopotentials[63] for all the elements were used with the generalized gradient approximation (GGA)[64] for exchange-correlation corrections. A split-valence double-ζ basis set was used for all atoms where polarization orbitals were included as obtained with an energy shift of 0.1 eV. The energy cutoff of the real space integration mesh was 300 Ry. A 6 × 4 × 4 Monkhorst−Pack (MP)[65] mesh was used for sampling the Brillouin zone. A self-consistency was achieved within the total energy change less than 10^{-4} eV. The experimental crystal structures were adapted for all calculations. Crystal orbital Hamilton population (COHP)[66] calculations were also performed using the NAOPP method after the total energy was self-consistently achieved.

Electron localization function (ELF)[67,68] calculations were performed using the PWPP method. Norm-conserving MT pseudopotentials for all the elements were used with the GGA for exchange-correlation corrections. The pseudopotentials generated from the Fritz Haber Institute (FHI) code were converted for the calculations.[69] A plane wave energy cutoff was set to 37 Ry. The Brillouin zone was sampled using a 6 × 4 × 4 MP k-point grid. A total energy convergence threshold was set to 10^{-6} Ry indicated self-consistency. The experimental crystal structures were employed for all calculations.

A hypothetical structure, $Zn_2(MoO_4)(SO_3)$, was obtained using the PWPP method in order to systematically study the electronic structures of $Zn_2(MoO_4)(AO_3)$ (A = S^{4+}, Se^{4+}, and Te^{4+}). Initially, the structure of $Zn_2(MoO_4)(SO_3)$ was adapted to the structure of $Zn_2(MoO_4)(SeO_3)$ where Se is replaced by S. Structural optimization was employed with the GGA for the exchange-correlation corrections. The experimental symmetry of $Zn_2(MoO_4)(SeO_3)$ was retained during the relaxation. The Hellmann−Feynman force and the total energy changes were set to 10^{-3} Ry per atomic unit (a.u.) and 10^{-4} Ry, respectively, between two consecutive self-consistent field steps. A plane wave energy cutoff was set to 37 Ry. For all of the structural figures and electronic structure results, the program VESTA was used.[70]

RESULTS AND DISCUSSION

Structures. $Zn_2(MoO_4)(AO_3)$ (A = Se^{4+} or Te^{4+}) represent two new polar oxide materials. The isostructural compounds exhibit three-dimensional crystal structures that contain ZnO_4, ZnO_6, MoO_4, and AO_3 polyhedra (see Figure 1). There are two crystallographically unique zinc sites, hereafter Zn(1) and Zn(2), that have tetrahedral and octahedral coordination environments respectively. The ZnO_4 tetrahedra share edges with an AO_3 polyhedron and a ZnO_6 octahedron, and share corners with an additional AO_3 polyhedron, ZnO_6 octahedron, and MoO_4 tetrahedron. This complex connectivity results in the three-dimensional crystal network (see Figure 2). In connectivity terms, the structure may be written as $\{[AO_{3/3}]^{2+}[MoO_{4/2}]^{2+}[ZnO_{1/2}O_{3/3}]^{1-}[ZnO_{3/3}O_{3/2}]^{3-}\}^0$. For $Zn_2(MoO_4)(SeO_3)$ ($Zn_2(MoO_4)(TeO_3)$), the Zn(1)−O, Zn(2)−O, Mo−O, and Se−O(Te−O) bond distances are in the range of 1.963(5)−2.002(3)(1.937(5)−1.998(5)) Å, 1.986(3)−2.227(3)(2.016(5)−2.181(5)) Å, 1.744(4)−1.789(3)(1.743(5)−1.790(5)) Å, and 1.705(3)−1.721(3)(1.882(5)−1.890(5)) Å, respectively (see Table 2). The bond valence calculations for Zn^{2+}, Mo^{6+}, and Se^{4+}(Te^{4+}) resulted in values 1.89−1.99, 5.87−5.97, and 3.89(3.83), respectively (see Table 3).

As stated earlier $Zn_2(MoO_4)(AO_3)$ (A = Se^{4+} or Te^{4+}) is found in the polar space group $P2_1$ (No. 4); thus, it is relevant to discuss the structural origin of the polarity. Only the Mo^{6+} and A^{4+} cations are amenable to SOJT distortions; however, a SOJT distortion is not observed in Mo^{6+} attributable to its tetrahedral coordination. Thus, only the A^{4+} cations undergo SOJT distortions. This distortion results in the formation of a stereoactive lone-pair that creates a locally asymmetric and polar AO_3 coordination environment (see Figure 1). The arrows in Figure 1 indicate the approximate direction of the local dipole moment on the AO_3 polyhedron. As seen, there is some "constructive addition" resulting in a net moment directed approximately toward the *b*-axis direction. We will be discussing the stereoactive lone-pair and its relevance to the observed functional properties,

dx.doi.org/10.1021/ic200511q |*Inorg. Chem.* 2011, 50, 5215–5222

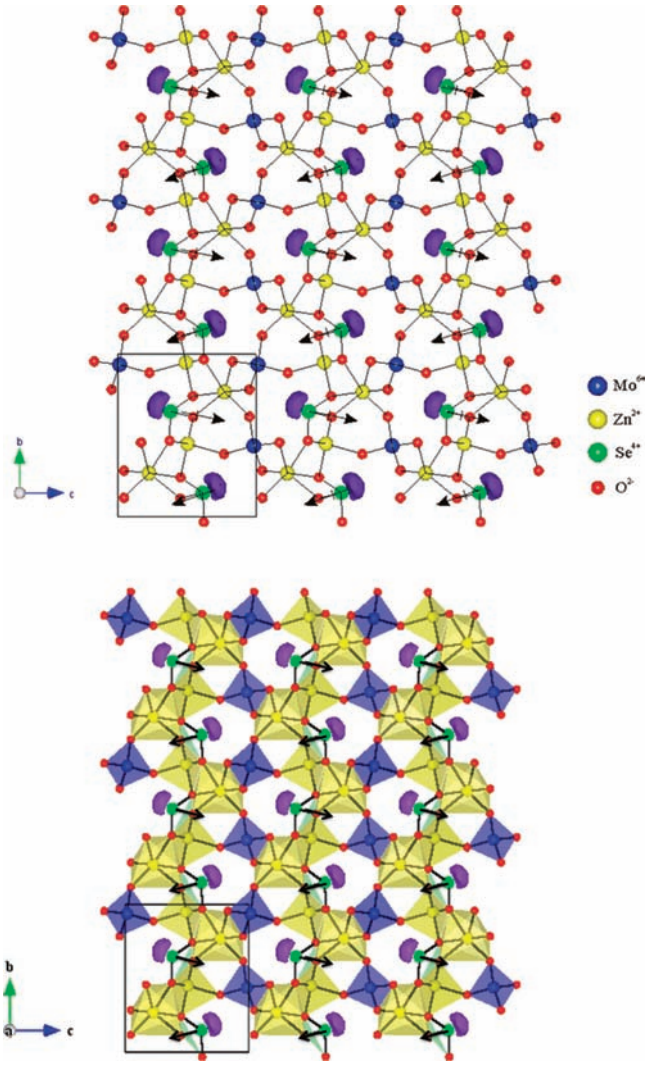

Figure 1. Ball-and-stick (top) and polyhedral (bottom) representation of $Zn_2(MoO_4)(SeO_3)$ in the *bc*-plane. The arrows indicate the approximate directions of the dipole moment on the SeO_3 polyhedron. Electron localization function (ELF) with $\eta = 0.9$ is shown, indicating that the lone-pair on the Se^{4+} is stereoactive.

that is, second-harmonic generation, pyroelectricity, and piezoelectricity, later in the paper.

IR Spectroscopy. The IR spectra for $Zn_2(MoO_4)(AO_3)$ (A = Se^{4+} or Te^{4+}) revealed absorption bands of Mo−O, Se(Te)−O vibrations in the 400−1000 cm^{-1} range. The Mo−O stretching vibrations were observed around 811−940 cm^{-1}, whereas Se(Te)−O stretching vibrations were seen around 673−750 cm^{-1}. The absorption band occurring below 650 cm^{-1} can be assigned to Mo−O−Se(Te) bending vibrations. These assignments are in good agreement with the literature.[71−73] The IR spectra and assignments were deposited in the Supporting Information (see Figure S2).

UV−vis Diffuse Reflectance Spectroscopy. Reflectance spectra of $Zn_2(MoO_4)(AO_3)$ (A = Se^{4+} or Te^{4+}) were converted to absorbance using the Kubelka−Munk function:

$$F(R) = (1 - R)^2/2R = K/S$$

where *R*, *K*, and *S* represent the reflectance, the absorption, and the scattering, respectively. In a $F(R)$ versus E (eV) plot,

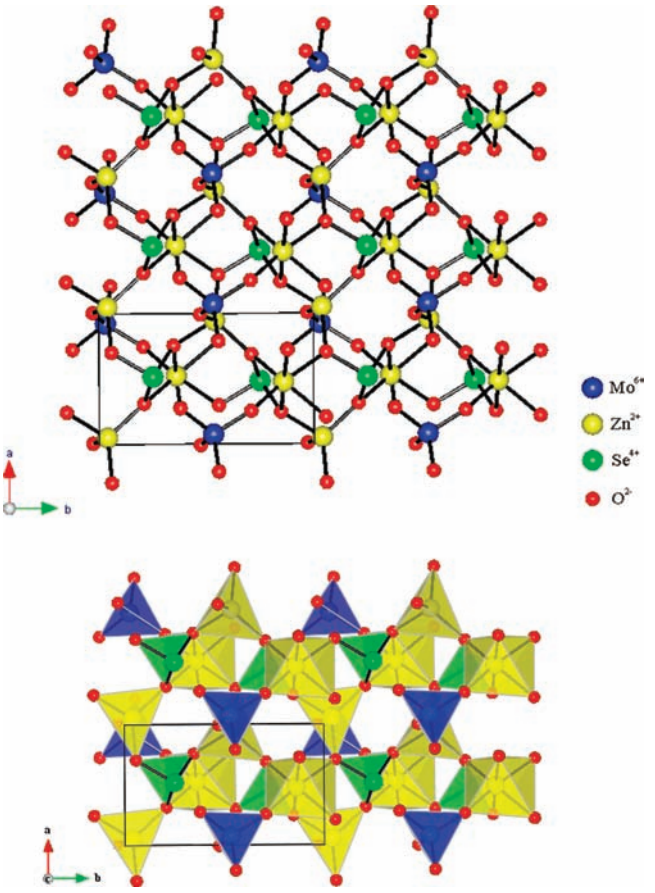

Figure 2. Ball-and-stick (top) and polyhedral (bottom) diagram of $Zn_2(MoO_4)(SeO_3)$ in the *ab*-plane. Note that the polyhedra share edges and corners resulting in the three-dimensional crystal structure.

extrapolating the linear part of the rising curve to zero provides onset absorption of 4.2 and 4.1 eV for $Zn_2(MoO_4)(SeO_3)$ and $Zn_2(MoO_4)(TeO_3)$, respectively. These values are in good agreement with the energy gap obtained from their calculated electronic band structures, as well as consistent with the colorless nature of the materials. For these materials, the top of the valence band mainly consists of O-2sp orbitals, whereas the bottom of the conduction band is mainly composed of contribution from Mo-4d (see Figure 3). Thus, the optical band gap is mainly attributable to ligand-to-metal, O-2sp to Mo-4d, charge transfer.[74,75] The UV−vis diffuse reflectance spectra for the reported compounds were deposited in the Supporting Information (see Figure S3).

Thermal Analysis. The thermal stability of $Zn_2(MoO_4)(AO_3)$ (A = Se^{4+} or Te^{4+}) were investigated through thermogravimetric and differential thermal analyses (TGA and DTA) (see Figure S4, Supporting Information). The TGA and DTA data of $Zn_2(MoO_4)(SeO_3)$ indicated that the oxide releases SeO_2 at ~500 °C and subsequently decomposes to ZnO, $ZnMoO_4$, and $Zn_3Mo_2O_9$ (see Figure S5, Supporting Information). The TGA and DTA data of $Zn_2(MoO_4)(TeO_3)$ revealed that the oxide melts congruently at approximately 831 °C. As seen in the TGA data, no weight loss was observed in the range of 25−850 °C, but the DTA data revealed an endothermic (exothermic) peak around 831 °C (817 °C) in the heating (cooling) cycle. Also, the PXRD pattern of the melted $Zn_2(MoO_4)(TeO_3)$ sample is consistent with the as-synthesized $Zn_2(MoO_4)(TeO_3)$ (see Figure S5, Supporting Information).

Table 3. Bond Valence Sum (BVS), Bond Strain Index (BSI), Global Instability Index (GII), Unit Cell Dipole Moment (μ), SHG Efficiencies ($\times$ α-SiO_2), Piezoelectric Responses, (d_{33}), Pyroelectric Coefficients (P_T) and Maximum Polarization (P_m) for $Zn_2(MoO_4)(AO_3)$ (A = Se^{4+} or Te^{4+})

	BVS[a]							functional properties			
	$Zn(1)^{2+}$	$Zn(2)^{2+}$	A^{4+}	Mo^{6+}	BSI[a]	GII[a]	μ[b]	SHG	d_{33}[c]	P_T[d]	P_m[e]
$Zn_2(MoO_4)(SeO_3)$	1.89	1.99	3.89	5.97	0.110	0.077	16.5	100	14	−0.31	0.034
$Zn_2(MoO_4)(TeO_3)$	1.98	1.98	3.83	5.87	0.096	0.101	14.2	80	30	−0.64	0.060

[a] Valence unit (vu). [b] Debye. [c] pm/V. [d] At 55 °C ($\mu C/m^2$ K). [e] At 100 Hz ($\mu C/cm^2$).

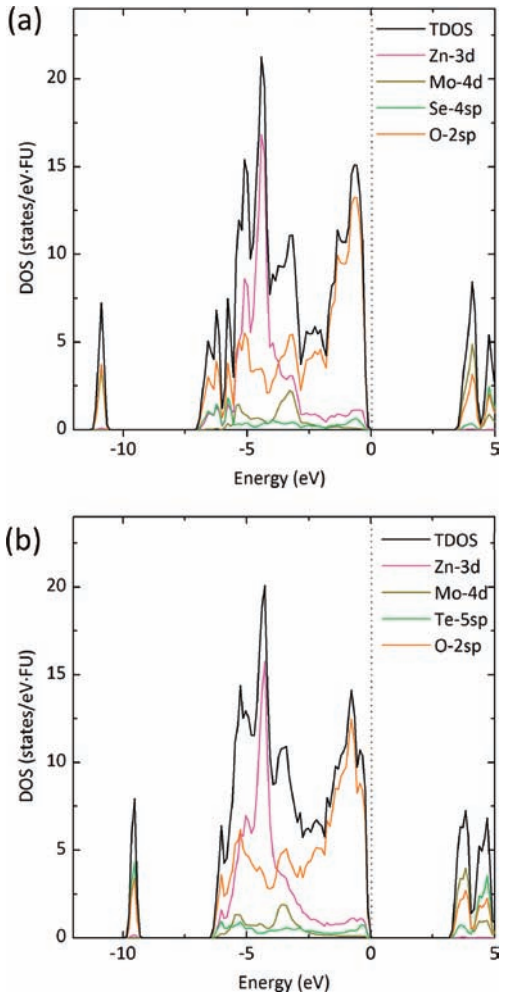

Figure 3. Total and projected density of states plots for (a) $Zn_2(MoO_4)(SeO_3)$ and (b) $Zn_2(MoO_4)(TeO_3)$. The dotted vertical line at 0 eV indicates E_F.

Second Harmonic Generation. Powder SHG measurements in the particle size range of 25−120 μm indicated that $Zn_2(MoO_4)(AO_3)$ (A = Se^{4+} or Te^{4+}) are nonphase matching with comparable efficiencies. Their powder SHG efficiencies were ∼100 × and ∼80 × α-SiO_2 in the particle size range of 45−63 μm for $Zn_2(MoO_4)(SeO_3)$ and $Zn_2(MoO_4)(TeO_3)$, respectively. These indicate $Zn_2(MoO_4)(SeO_3)$ and $Zn_2(MoO_4)(TeO_3)$ fall into the class C of SHG materials as defined by Kurtz and Perry.[55] The average NLO susceptibilities, $<d_{eff}>_{exp}$, can be estimated to be ∼5.79 pm/V and ∼4.78 pm/V, respectively (see Figure S6, Supporting Information).[2] The moderate SHG efficiencies are attributable to the partial alignment of the AO_3 polyhedra (see Figure 1). As seen in Figure 1, the moments associated with the AO_3 polyhedra are not parallel. In fact, the moments are only partially aligned. This partial "constructive addition" results in the observed moderate SHG efficiencies of ∼100 × and ∼80 × α-SiO_2 for $Zn_2(MoO_4)(SeO_3)$ and $Zn_2(MoO_4)(TeO_3)$ respectively.

Piezoelectricity Measurements. Converse piezoelectric measurements were performed on $Zn_2(MoO_4)(AO_3)$ (A = Se^{4+} or Te^{4+}) at room temperature. With each sample, a voltage of 2000 V at 50 Hz was applied. The d_{33} piezoelectric charge constants, which is defined as the ratio between the strain produced and the electrical voltage applied, for $Zn_2(MoO_4)(SeO_3)$ and $Zn_2(MoO_4)(TeO_3)$ were estimated to be 14.1 and 30.0 pm/V, respectively. The piezoelectric data were deposited in the Supporting Information (see Figure S7).

POLARIZATION MEASUREMENTS

The reported materials are not only NCS but also are polar — a macroscopic dipole moment is observed. The macroscopic polarity suggests the possibility for ferroelectric behavior. Ferroelectric hysteresis measurements were performed on pressed pellets, and polarization loops were observed. In addition, these loops did appear to exhibit frequency dependence (see Figures S8 and S9, Supporting Information). However, these loops are not attributable to ferroelectric hysteresis, that is, the reported materials are not ferroelectric — the macroscopic polarization cannot be reversed in the presence of an external electric field. It has been demonstrated that these types of loops have been erroneously attributed to ferroelectric behavior.[76] With the reported materials, it is important to understand why the materials, although polar, are not ferroelectric. As stated earlier, for ferroelectric behavior to occur the macroscopic polarization must be switchable in the presence of an external electric field. This implies that the local moments must also be reversed. In $Zn_2(MoO_4)(AO_3)$ (A = Se^{4+} or Te^{4+}), only the SeO_3 and TeO_3 polyhedra exhibit a local dipole moment. Thus, it is these dipole moments that must be reversed for ferroelectric behavior to occur. We have already shown that the energy barrier to inversion a SeO_3 polyhedron is ∼5.3 eV,[46] which is substantially larger than what is observed in ferroelectric $BaTiO_3$ (1.8×10^{-2} eV) and $PbTiO_3$ (2.0×10^{-1} eV).[77] Preliminary calculations suggest that the barrier to inversion for a TeO_3 polyhedron is nearly 7 eV. Thus, polarization reversal in $Zn_2(MoO_4)(AO_3)$ (A = Se^{4+} or Te^{4+}) is energetically very unfavorable, rendering the materials nonferroelectric. The materials are, however, pyroelectric.

Pyroelectric measurements were performed by measuring the spontaneous polarization (P_S) as a function of temperature. The values of the pyroelectric coefficient, which is defined as dP/dT,

dx.doi.org/10.1021/ic200511q |Inorg. Chem. 2011, 50, 5215–5222

for $Zn_2(MoO_4)(SeO_3)$ and $Zn_2(MoO_4)(TeO_3)$ at 55 °C are −0.31 and −0.64 $\mu C/m^2$ K, respectively. The polarization data were deposited in the Supporting Information (see Figures S8 and S9).

Electronic Band Structures. The electronic band structures of $Zn_2(MoO_4)(AO_3)$ (A = Se^{4+} or Te^{4+}) were performed using the NAOPP method. The total density of states (TDOS) and projected density of states (PDOSs) of both materials are shown in Figure 3 where an energy gap of 3.3 and 3.1 eV reveals at the Fermi level (E_F) for $Zn_2(MoO_4)(SeO_3)$ and $Zn_2(MoO_4)(TeO_3)$, respectively. The energy gaps indicate their insulating nature that is consistent with the observed energy gaps of 4.2 and 4.1 eV observed in the UV−vis diffuse reflectance spectra of $Zn_2(MoO_4)(SeO_3)$ and $Zn_2(MoO_4)(TeO_3)$, respectively.[78−80] Overall, their electronic structures are similar because the materials are isostructural. As seen in Figure 3, narrow and broad valence bands that are separated by approximately 3 eV are shown near −10 eV and −7 eV relative to E_F. The PDOSs indicate that the narrow band consists of almost equal amounts of O-2s and Se-4s(Te-5s) contributions. The broad band has contributions from O-2sp, Zn-3d, Mo-4d, and Se-4sp(Te-5sp). As seen in PDOSs, the bottom part of the band (∼ −7 eV to ∼ −6 eV) is mostly contributed by O-2sp and Se-4p(Te-5p), and the middle part of the band (∼ −6 eV to ∼ −2.5 eV) is composed of mainly Zn-3d and O-2sp, and the top part of the band (∼ −2.5 eV to E_F) consists of mostly O-2sp. In fact, the bottom part of the band indicates Se(Te)−O interactions where three DOS peaks and one peak shown in each DOSs of $Zn_2(MoO_4)(SeO_3)$ and $Zn_2(MoO_4)(TeO_3)$ are mainly attributable to the differences in the Se−O and Te−O bond lengths (see Table 2). The middle part of the band indicates a weak interaction between O-2sp and Zn-3d, consistent with the ionic character of the $Zn^{2+}(3d^{10})$ cations. The top part of the band is indicative of the nonbonding character of O-2sp. However, a relatively small contribution of Se-4sp or Te-5sp is observed directly below the E_F in both electronic structures as seen in Figure S10, Supporting Information that is associated with their lone-pair formation on Se^{4+} or Te^{4+} cations, respectively. In order to gain insight into how their lone-pair electrons are formed, the crystal orbital Hamilton population (−COHPs) were calculated for Se(Te−O) interactions utilizing the NAOPP method. In Figure S11, Supporting Information, the −COHP curves for Se−O and Te−O interactions are similar overall and reveal the antibonding character near the E_F. There is, however, a major difference. If the narrow band states in the −COHP and PDOS are examined more closely, that is, the bands near −10 eV relative to E_F, we observe that for −COHP(narrow band)/PDOS(narrow band) the Te−O interactions are much weaker compared with the Se−O interactions. Their similar DOSs and −COHPs, specifically the antibonding character of Se(Te)−O near the E_F for both materials, raise a relevant question, "Are the driving forces similar or different for the stereo-active lone-pair formation on Se^{4+} and Te^{4+} cations?" In other words, which mechanism, sp-mixing on the cations alone or sp-mixing on the cations with the oxygen orbitals, is favorable for stereoactive lone-pair formation with each cation? In order to address these issues, we thought it would be relevant to examine structural and electronic aspects of SO_3, SeO_3, and TeO_3 trigonal pyramids. Thus, a hypothetical electronic band structure for $Zn_2(MoO_4)(SO_3)$ was calculated with its optimized structure (see Computational Details and Figure S12, Supporting Information). As anticipated, the TDOS and PDOSs for $Zn_2(MoO_4)(SO_3)$ are very similar to $Zn_2(MoO_4)(SeO_3)$ and $Zn_2(MoO_4)(TeO_3)$. In spite of the similarities, there are differences in the electronic and structural aspects — the relative contribution of S-3s, Se-4s, and Te-5s in the PDOSs, the relative strength of S−O, Se−O and Te−O interactions in the narrow band in the −COHPs analyses, and a change in the O−A−O angle of the AO_3 trigonal pyramids, respectively. As seen in the PDOSs, the contributions of the s-orbital of the A cations *increase* from S to Se to Te, whereas the relative strengths of the A−O interactions *decrease* from S to Se to Te. These electronic differences indicate the s-orbital becomes localized going from S to Se to Te. This is consistent with earlier observations.[81,82] In fact, with the overall electronic aspects, $Zn_2(MoO_4)(SeO_3)$ is much more similar to $Zn_2(MoO_4)(SO_3)$ compared with $Zn_2(MoO_4)(TeO_3)$. Thus, sp-mixing of the A cations decrease from S and Se to Te. With the structural aspects, the O−A−O angles decrease from 101.4° to 97.6(2)° to 93.1(2)° for A = S^{4+}, Se^{4+}, and Te^{4+}, respectively (see Table 4). This reduction in the O−A−O angle indicates greater localization of the A-s orbital and strength of the A−O interaction. Consequently, both electronic and structural aspects indicate that the formation of the stereoactive lone-pair is similar for the S^{4+} and Se^{4+} cations but different compared with the Te^{4+} cation. The lone-pair formation on the S^{4+} and Se^{4+} cations are mainly attributable to the sp-mixing on the cations alone, whereas for the Te^{4+} cation the stereoactive lone-pair is attributable to cation sp-mixing through Te−O interactions.[82] Despite the different origins for the lone-pair formation, the antibonding character of A−O bonds appears near the E_F, as a result of the relatively lower energy levels of Se-4s(Te-5s) than that of O-2p with the valence state of Se($4s^2 4p^0$)(Te($5s^2 5p^0$)).

Table 4. Bond Angles for the Asymmetric AO_3 Trigonal Pyramids in $Zn_2(MoO_4)(AO_3)$ (A = S^{4+}, Se^{4+}, and Te^{4+})[a]

compound	bond angle (°)	
$Zn_2(MoO_4)(SO_3)$	∠O(1)−S−O(2)	103.5
	∠O(2)−S−O(4)	94.2
	∠O(1)−S−O(4)	106.5
	avg	**101.4**
$Zn_2(MoO_4)(SeO_3)$	∠O(1)−Se−O(2)	98.0(2)
	∠O(2)−Se−O(4)	92.2(2)
	∠O(1)−Se−O(4)	102.9(2)
	avg	**97.6(2)**
$Zn_2(MoO_4)(TeO_3)$	∠O(1)−Te−O(2)	94.1(2)
	∠O(2)−Te−O(4)	85.9(2)
	∠O(1)−Te−O(4)	99.2(2)
	avg	**93.1(2)**

[a] Note that the structure of $Zn_2(MoO_4)(SO_3)$ is hypothetical.

To better examine and understand the lone-pair characteristics on the Se^{4+} and Te^{4+} cations, electron localization function (ELF) calculations were performed using the PWPP method. Figure 1 shows the ELF iso-surface for η = 0.9 where, as anticipated, a lobe-like iso-surface is observed near the A^{4+} cation. This iso-surface may be considered as a stereoactive lone-pair.

CONCLUSION

Two new isostructural polar oxide materials, $Zn_2(MoO_4)(SeO_3)$ and $Zn_2(MoO_4)(TeO_3)$, have been synthesized and characterized. The materials exhibit three-dimensional crystal

structures consisting of ZnO_4, ZnO_6, MoO_4, and AO_3 ($A = Se^{4+}$ or Te^{4+}) polyhedra. The polarity of the materials may be structurally derived from the partial alignment of the NCS and polar AO_3 polyhedra. Attributable to this partial alignment, Moderate SHG efficiencies of 100 × and 80 × α-SiO_2 for $Zn_2(MoO_4)(SeO_3)$ and $Zn_2(MoO_4)(TeO_3)$, respectively, are observed. Although the materials exhibit macroscopic polarization, the materials are not ferroelectric as the polarization is not reversible. Interestingly, DTA measurements indicate that $Zn_2(MoO_4)(TeO_3)$ melts congruently suggesting that large crystal growth is possible. We are currently investigating this possibility.

■ ASSOCIATED CONTENT

Supporting Information. X-ray crystallographic files in CIF format, experimental and calculated powder X-ray diffraction patterns, infrared and UV−vis spectra, thermogravimetric and differential thermal analysis diagrams, piezoelectric and polarization-electric loops for $Zn_2(MoO_4)(AO_3)$ ($A = Se^{4+}$ or Te^{4+}) with density of states, bond analysis, and crystal structures of hypothetical structure of $Zn_2(MoO_4)(SO_3)$. These materials are available free of charge via the Internet at http://pubs.acs.org.

■ AUTHOR INFORMATION

Corresponding Author
*E-mail: psh@uh.edu.

■ ACKNOWLEDGMENT

We thank the Robert A. Welch Foundation (Grant E-1457), the Texas Center for Superconductivity, and the NSF (DMR-0652150) for support. Sau Nguyen thanks the Vietnam Government for an opportunity to study at the University of Houston.

■ REFERENCES

(1) Lang, S. B. *Phys. Today* **2005**, *58*, 31.
(2) Ok, K. M.; Chi, E. O.; Halasyamani, P. S. *Chem. Soc. Rev.* **2006**, *35*, 710.
(3) Khomskii, D. I. *Physics* **2009**, 2.
(4) Lang, S. B.; Das-Gupta, D. K. In *Handbook of Advanced Electronic and Photonic Materials and Devices*; Hari Singh, N., Eds.; Academic Press: Burlington, 2001; p 1.
(5) *International Tables for Crystallography, Vol. A, Space Group Symmetry*; Hahn, T., Ed.; Kluwer Academic: Dordrecht, Holland, 2006; Vol. A.
(6) Lines, M. E.; Glass, A. M. *Principles and Applications of Ferroelectrics and Related Materials*; Oxford University Press: Oxford, 1991.
(7) Zhang, S.-Y.; Jiang, H.-L.; Sun, C.-F.; Mao, J.-G. *Inorg. Chem.* **2009**, *48*, 11809.
(8) Heier, K. R.; Norquist, A. J.; Halasyamani, P. S.; Duarte, A.; Stern, C. L.; Poeppelmeier, K. R. *Inorg. Chem.* **1999**, *38*, 762.
(9) Welk, M. E.; Norquist, A. J.; Stern, C. L.; Poeppelmeier, K. R. *Inorg. Chem.* **2000**, *39*, 3946.
(10) Welk, M. E.; Norquist, A. J.; Stern, C. L.; Poeppelmeier, K. R. *Inorg. Chem.* **2001**, *40*, 5479.
(11) Welk, M. E.; Norquist, A. J.; Arnold, F. P.; Stern, C. L.; Poeppelmeier, K. R. *Inorg. Chem.* **2002**, *41*, 5119.
(12) Izumi, H. K.; Kirsch, J. E.; Stern, C. L.; Poeppelmeier, K. R. *Inorg. Chem.* **2005**, *44*, 884.
(13) Marvel, M. R.; Lesage, J.; Baek, J.; Halasyamani, P. S.; Stern, C. L.; Poeppelmeier, K. R. *J. Am. Chem. Soc.* **2007**, *129*, 13963.
(14) Kong, F.; Huang, S.-P.; Sun, Z.-M.; Mao, J.-G.; Cheng, W.-D. *J. Am. Chem. Soc.* **2006**, *128*, 7750.
(15) Jiang, H.-L.; Huang, S.-P.; Fan, Y.; Mao, J.-G.; Cheng, W.-D. *Chem.—Eur. J.* **2008**, *14*, 1972.
(16) Hu, T.; Qin, L.; Kong, F.; Zhou, Y.; Mao, J.-G. *Inorg. Chem.* **2009**, *48*, 2193.
(17) Sun, C.-F.; Hu, C.-L.; Xu, X.; Ling, J.-B.; Hu, T.; Kong, F.; Long, X.-F.; Mao, J.-G. *J. Am. Chem. Soc.* **2009**, *131*, 9486.
(18) Do, J.; Kanatzidis, M. G. *J. Alloys Compd.* **2004**, *381*, 41.
(19) Banerjee, S.; Malliakas, C. D.; Jang, J. I.; Ketterson, J. B.; Kanatzidis, M. G. *J. Am. Chem. Soc.* **2008**, *130*, 12270.
(20) Chung, I.; Song, J.-H.; Jang, J. I.; Freeman, A. J.; Ketterson, J. B.; Kanatzidis, M. G. *J. Am. Chem. Soc.* **2009**, *131*, 2647.
(21) Chung, I.; Jang, J.-I.; Malliakas, C. D.; Ketterson, J. B.; Kanatzidis, M. G. *J. Am. Chem. Soc.* **2010**, *132*, 384.
(22) Bera, T. K.; Jang, J. I.; Song, J.-H.; Malliakas, C. D.; Freeman, A. J.; Ketterson, J. B.; Kanatzidis, M. G. *J. Am. Chem. Soc.* **2010**, *132*, 3484.
(23) Jiang, H.-L.; Xie, Z.; Mao, J.-G. *Inorg. Chem.* **2007**, *46*, 6495.
(24) Opik, U.; Pryce, M. H. L. *Proc. R. Soc. London, Ser. A* **1957**, *238*, 425.
(25) Bader, R. F. W. *Mol. Phys.* **1960**, *3*, 137.
(26) Bader, R. F. W. *Can. J. Chem.* **1962**, *40*, 1164.
(27) Pearson, R. G. *J. Am. Chem. Soc.* **1969**, *91*, 4947.
(28) Pearson, R. G. *J. Mol. Struct.: THEOCHEM* **1983**, *103*, 25.
(29) Wheeler, R. A.; Whangbo, M. H.; Hughbanks, T.; Hoffmann, R.; Burdett, J. K.; Albright, T. A. *J. Am. Chem. Soc.* **1986**, *108*, 2222.
(30) Kunz, M.; Brown, I. D. *J. Solid State Chem.* **1995**, *115*, 395.
(31) Goodenough, J. B. *Annu. Rev. Mater. Sci.* **1998**, *28*, 1.
(32) Halasyamani, P. S.; Poeppelmeier, K. R. *Chem. Mater.* **1998**, *10*, 2753.
(33) Izumi, H. K.; Kirsch, J. E.; Stern, C. L.; Poeppelmeier, K. R. *Inorg. Chem.* **2005**, *44*, 884.
(34) Marvel, M. R.; Pinlac, R. A. F.; Lesage, J.; Stern, C. L.; Poeppelmeier, K. R. *Z. Anorg. Allg. Chem.* **2009**, *635*, 869.
(35) Goodey, J.; Broussard, J.; Halasyamani, P. S. *Chem. Mater.* **2002**, *14*, 3174.
(36) Ra, H.-S.; Ok, K. M.; Halasyamani, P. S. *J. Am. Chem. Soc.* **2003**, *125*, 7764.
(37) Ok, K. M.; Halasyamani, P. S. *Angew. Chem., Int. Ed.* **2004**, *43*, 5489.
(38) Chi, E. O.; Ok, K. M.; Porter, Y.; Halasyamani, P. S. *Chem. Mater.* **2006**, *18*, 2070.
(39) Sivakumar, T.; Ok, K. M.; Halasyamani, P. S. *Inorg. Chem.* **2006**, *45*, 3602.
(40) Kim, J.-H.; Baek, J.; Halasyamani, P. S. *Chem. Mater.* **2007**, *19* 5637.
(41) Chang, H. Y.; Sivakumar, T.; Ok, K. M.; Halasyamani, P. S. *Inorg. Chem.* **2008**, *47*, 8511.
(42) Kim, Y.; Seo, I.-s.; Martin, S. W.; Baek, J.; Halasyamani, P. S.; Arumugam, N.; Steinfink, H. *Chem. Mater.* **2008**, *20*, 6048.
(43) Chang, H. Y.; Kim, S.-H.; Ok, K. M.; Halasyamani, P. S. *Chem. Mater.* **2009**, *21*, 1654.
(44) Chang, H.-Y.; Kim, S.-H.; Halasyamani, P. S.; Ok, K. M. *J. Am. Chem. Soc.* **2009**, *131*, 2426.
(45) Chang, H.-Y.; Kim, S.-H.; Ok, K. M.; Halasyamani, P. S. *J. Am. Chem. Soc.* **2009**, *131*, 6865.
(46) Kim, S.-H.; Yeon, J.; Halasyamani, P. S. *Chem. Mater.* **2009**, *21*, 5335.
(47) Chang, H. Y.; Kim, S. H.; Halasyamani, P. S. *Chem. Mater.* **2010**, *22*, 3241.
(48) *SAINT, Program for Area Detector Absorption Correction*, version 4.05; Siemens Analytical X-ray Systems, Inc.: Madison, WI, 1995.
(49) Sheldrick, G. M. *SHELXS-97 - A program for Automatic Solution of Crystal Structures*; University of Goettingen: Goettingen, Germany, 1997.
(50) Sheldrick, G. M. *SHELXL-97 - A Program for Crystal Structure Refinement*; University of Goettingen: Goettingen, 1997.
(51) Farrugia, L. J. *J. Appl. Crystallogr.* **1999**, *32*, 837.
(52) Spek, A. L. *PLATON*; Utrecht University: Utrecht, The Netherlands, 2001.

(53) Kubelka, P.; Munk, F. *Z. Tech. Phys.* **1931**, *12*, 593.
(54) Tauc, J. *Mater. Res. Bull.* **1970**, *5*, 721.
(55) Kurtz, S. K.; Perry, T. T. *J. Appl. Phys.* **1968**, *39*, 3798.
(56) Hohenberg, P.; Kohn, W. *Phys. Rev.* **1964**, *136*, B864.
(57) Kohn, W.; Sham, L. J. *Phys. Rev.* **1965**, *140*, A1133.
(58) Junquera, J.; Paz, O.; Sanchez-Portal, D.; Artacho, E. *Phys. Rev. B* **2001**, *64*, 235111/1.
(59) José, M. S.; *J. Phys.: Condens. Matter* **2002**, *14*, 2745.
(60) Ordejón, P.; Artacho, E.; Soler, J. M. *Phys. Rev. B* **1996**, *53*, R10441.
(61) Torres, J. A.; Artacho, E.; Cela, J. M.; Gale, J.; García, A.; Junquera, J.; Martin, R. M.; Ordejón, P.; Sánchez, D.; Soler, J. M. *SIESTA-3.0-rc2*; http://www.icmab.es/siesta/, 2010.
(62) Baroni, S.; Corso, A. D.; Gironcoli, S. d.; Giannozzi, P.; Cavazzoni, C.; Ballabio, G.; Scandolo, S.; Chiarotti, G.; Focher, P.; Pasquarello, A.; Laasonen, K.; Trave, A.; Car, R.; Marzari, N.; Kokalj, A. *Quantum-ESPRESSO* Version 4.1.2 ed.; http://www.quantum-espresso.org/, 2009.
(63) Troullier, N.; Martins, J. L. *Phys. Rev. B: Condens. Matter* **1991**, *43*, 1993.
(64) Perdew, J. P.; Burke, K.; Ernzerhof, M. *Phys. Rev. Lett.* **1996**, *77*, 3865.
(65) Monkhorst, H. J.; Pack, J. D. *Phys. Rev. B* **1976**, *13*, 5188.
(66) Dronskowski, R.; Bloechl, P. E. *J. Phys. Chem.* **1993**, *97*, 8617.
(67) Becke, A. D.; Edgecombe, K. E. *J. Chem. Phys.* **1990**, *92*, 5397.
(68) Silvi, B.; Savin, A. *Nature* **1994**, *371*, 683.
(69) http://www.fhi-berlin.mpg.de/th/fhi98md/fhi98PP/, 2004.
(70) Momma, K.; Izumi, F. *J. Appl. Crystallogr.* **2008**, *41*, 653.
(71) Zhang, S.-Y.; Hu, C.-L.; Sun, C. F.; Mao, J.-G. *Inorg. Chem.* **2010**, *49*, 11627.
(72) Li, P.-X.; Kang, F.; Hu, C.-L.; Zhao, N.; Mao, J.-G. *Inorg. Chem.* **2010**, *49*, 5943.
(73) Zhang, S.-Y.; Jiang, H.-L.; Sun, C. F.; Mao, J.-G. *Inorg. Chem.* **2009**, *48*, 11809.
(74) Cotton, F. A.; Wilkinson, G.; Bochmann, M.; Murillo, C. *Advanced Inorganic Chemistry*, 6th ed.; Wiley: New York, 1998.
(75) Yeon, J.; Kim, S.-H.; Halasyamani, P. S. *Inorg. Chem.* **2010**, *49*, 6986.
(76) Scott, J. F. *J. Phys.: Condens. Matter* **2008**, *20*, 021001.
(77) Cohen, R. E. *Nature (London)* **1992**, *358*, 136.
(78) Mizoguchi, H.; Eng, H. W.; Woodward, P. M. *Inorg. Chem.* **2004**, *43*, 1667.
(79) Eng, H. W.; Barnes, P. W.; Auer, B. M.; Woodward, P. M. *J. Solid State Chem.* **2003**, *175*, 94.
(80) Mizoguchi, H.; Woodward, P. M. *Chem. Mater.* **2004**, *16*, 5233.
(81) Payne, D. J.; Egdell, R. G.; Walsh, A.; Watson, G. W.; Guo, J.; Glans, P. A.; Learmonth, T.; Smith, K. E. *Phys. Rev. Lett.* **2006**, *96*, 157403/1.
(82) Kim, M. K.; Kim, S.-H.; Chang, H.-Y.; Halasyamani, P. S.; Ok, K. M. *Inorg. Chem.* **2010**, *49*, 7028.